iScience

CellPress

Article

Target-Triggered Polymerization of Branched DNA Enables Enzyme-free and Fast Discrimination of Single-Base Changes

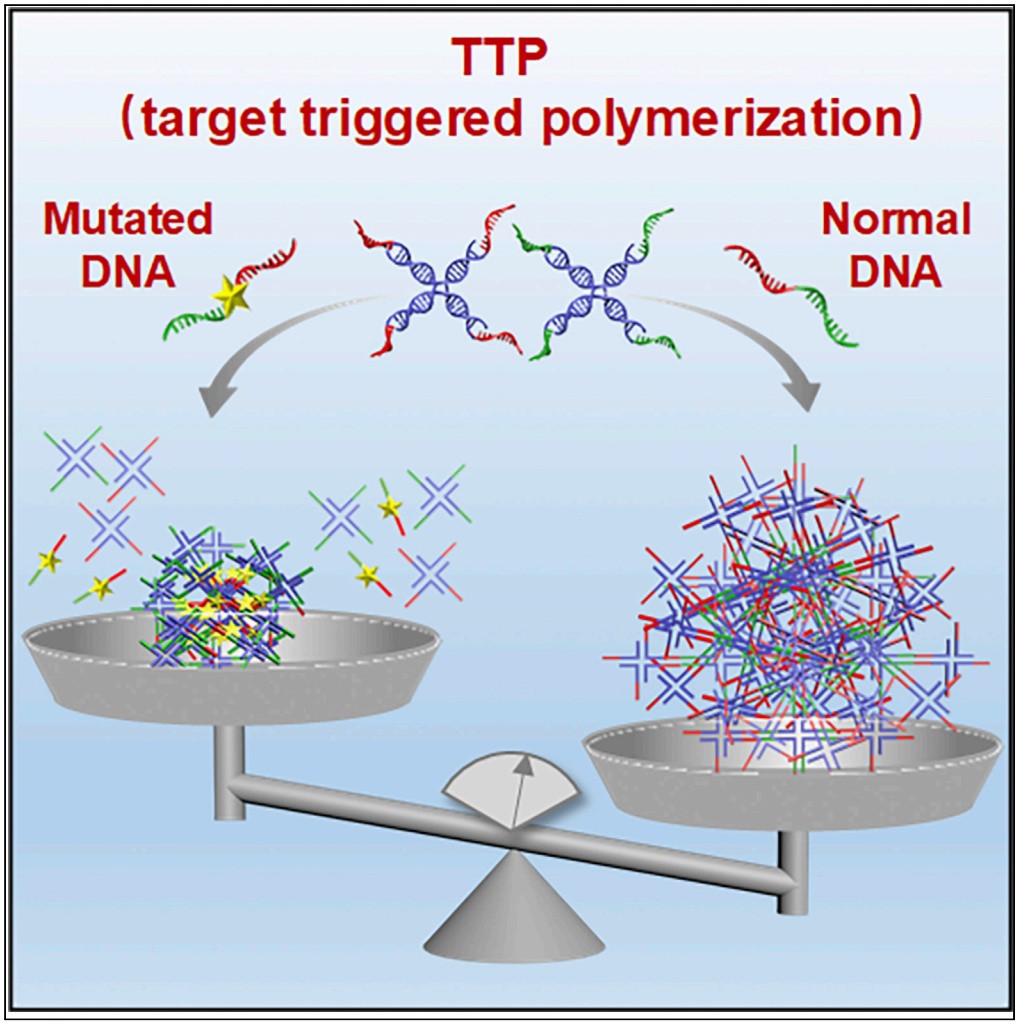

Yuhang Dong, Chi Yao, Zhi Wang, Dan Luo, Dayong Yang

dayong.yang@tju.edu.cn

HIGHLIGHTS

Enzyme-free, fast, and robust recognition of target DNA is realized

Discrimination of single-base-changing DNA from normal DNA is achieved

Different positions of single-base changes can be distinguished

A theoretical method is proposed for predicting hybridization probability

Dong et al., iScience *21*, 228–240
November 22, 2019
https://doi.org/10.1016/j.isci.2019.10.029

iScience

CellPress

Article

Target-Triggered Polymerization of Branched DNA Enables Enzyme-free and Fast Discrimination of Single-Base Changes

Yuhang Dong,[1,4] Chi Yao,[1,4] Zhi Wang,[1] Dan Luo,[2,3] and Dayong Yang[1,5,*]

SUMMARY

Single-base changes lead to important biological and biomedical implications; however, the discrimination of single-base changes from normal DNA always remains a grand challenge. Herein we developed a DNA recognition and amplification system based on artificial branched DNA, namely, target-triggered polymerization (TTP), to realize enzyme-free and fast discrimination of single-base changes. Branched DNA as monomers rapidly polymerized into DNA nanospheres only with the trigger of specific DNA. Our TTP system worked reliably over a wide range of conditions. Remarkably, our TTP system was capable of discriminating base-changing DNA from normal DNA, including distinguishing 1–4 nucleotide changes and positions of single base, which was attributed to the significant amplification of small differences in hybridization thermodynamics and kinetics. We further proposed a theoretical method for calculating the hybridization probability of nucleic acids, which performed highly consistent with experimental results.

INTRODUCTION

Nucleic acids are genetic biopolymers that are composed of nucleotides, which are essential to all known forms of life. Alteration of nucleotides between nucleic acid sequences (single-base substitution), as the most common form of nucleic acid variations, is often associated with important biological and biomedical implications (Sachidanandam et al., 2001; Smith et al., 2017). For instance, nucleotide changes in the coding region of genome affect the sequences of amino acid and protein function, leading to the occurrence of genetic disease (Lahiry et al., 2010; Sauna and Kimchi-Sarfaty, 2011). Nucleotide changes in the pathogen genome cause antibiotic resistance (Niemz et al., 2011). In addition, tumor-associated base changes have significant impacts on tumor growth, transformations, and metastasis, which can serve as noninvasive biomarkers of cancers (Greenman et al., 2007; Schwarzenbach et al., 2011). It is therefore vitally important to develop effective strategies for the discrimination of single-base changes (Chen et al., 2013).

Single-base changes have only one nucleotide difference with normal counterparts; it is extremely challenging to discriminate single-base-changing DNA from normal DNA because of the small energetic differences in hybridization reactions. DNA nanotechnology and the corresponding DNA nanostructures with recognition capability and programmability provide strategies for target recognition and signal amplification to increase the small differences (Huang et al., 2018; Zhao et al., 2015a; Zhou et al., 2018). Accordingly, DNA amplification technologies have been developed, such as polymerase chain reaction (PCR) (Khodakov et al., 2016), rolling circle amplification (Ali et al., 2014), loop-mediated amplification (Zhao et al., 2015a), enzyme-assisted target recycling (Gerasimova and Kolpashchikov, 2014), and hybridization chain reaction (HCR) (Chen et al., 2012; Huang et al., 2011; Xu et al., 2018). Despite the fact that these technologies have become promising, many challenges need to be addressed including complicated operation, time –consumption, and high cost owing to the involvement of enzymes. In addition, DNA nanostructures have been built as non-enzymatic tools for signal amplification. For example, DNA tetrahedron with highly rigid structures can effectively control the probes' density and orientation at the biosensor interfaces, enabling efficient hybridization and high sensitivity (Liu et al., 2018; Pei et al., 2010, 2014). Spherical nucleic acid conjugates possessing the periphery of high-dense nucleic acid probes and the core of inorganic nanoparticles are used as visible detection platform through color change generated by particle aggregation (Cutler et al., 2012; Rouge et al., 2015). Consequently, DNA nanostructures can serve as simultaneous target recognizer and signal amplifiers (Li et al., 2018), becoming effective elements for the discrimination of single-base changes (Hu et al., 2017). Given that the fine DNA nanostructure increased

[1]Frontier Science Center for Synthetic Biology, Key Laboratory of Systems Bioengineering (MOE), School of Chemical Engineering and Technology, Tianjin University, Tianjin 300350, P. R. China

[2]Department of Biological & Environmental Engineering, Cornell University, Ithaca, NY 14853, USA

[3]CAS Key Laboratory of Nano-Bio Interface, Suzhou Institute of Nano-Tech and Nano-Bionics, Chinese Academy of Sciences, Suzhou 215123, P. R. China

[4]These authors contributed equally

[5]Lead Contact

*Correspondence: dayong.yang@tju.edu.cn

https://doi.org/10.1016/j.isci.2019.10.029

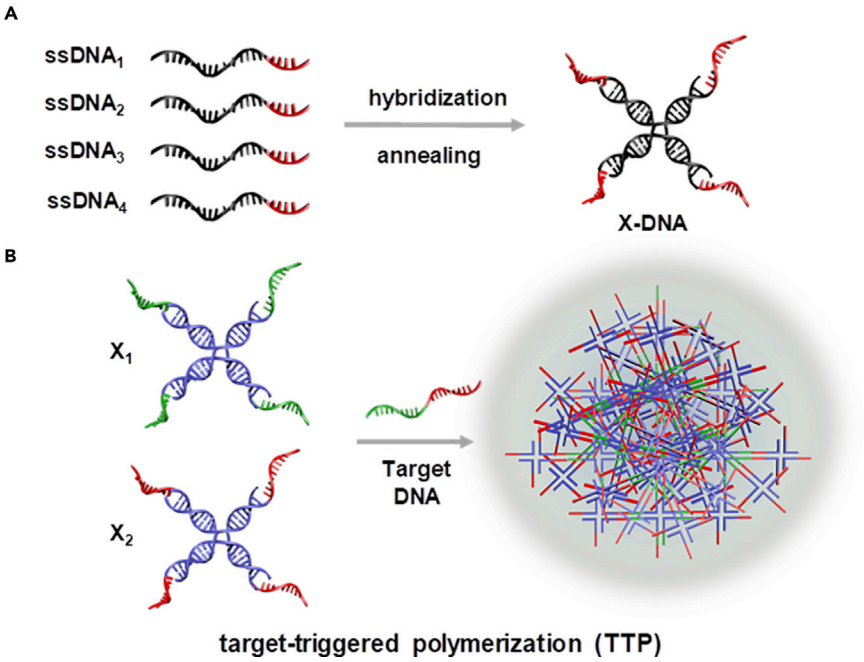

Scheme 1. Schematic Illustration of Enzyme-free and Fast Target-Triggered Polymerization (TTP) for Simultaneous Target Recognition and Signal Amplification

(A) Synthesis of X-shaped branched DNA (X-DNA) composed by four single-stranded DNA (ssDNA) through DNA hybridization and annealing procedure.

(B) Polymeric DNA nanosphere triggered by the self-assembly of X-DNA (X_1 and X_2) and target DNA (T-DNA).

the difficulty of design and use, it is necessary to develop an enzyme-free, simply designed, low-cost, and easily manipulated method for the discrimination of single-base changes.

Herein, we constructed a branched DNA-based polymerization system, namely, "target-triggered polymerization (TTP)." In TTP system, branched DNA was designed to polymerize into DNA nanospheres only under the trigger of specific DNA, realizing target recognition and efficient signal amplification simultaneously. Our TTP system can be accomplished rapidly without the involvement of any enzymes. In addition, the TTP system possessed robust performance in a wide range of conditions. Our enzyme-free, rapid, and robust TTP system enabled high specificity and sensitivity. Remarkably, our TTP system was capable of discriminating base-changing DNA from normal DNA, including different number of nucleotide changes and the positions of single-base change. Furthermore, thermodynamics and kinetics analyses showed that the TTP system apparently amplified the small differences of base-changing DNA with normal DNA in an identical hybridization reaction. Taking advantage of the TTP system, we developed a theoretical model for analyzing the hybridization probability of nucleic acids, which performed highly consistent with experimental results, making our TTP system a powerful tool for exploring the probability of nucleic acid hybridization.

RESULTS

Enzyme-free and Fast TTP System for Simultaneous Target Recognition and Signal Amplification

X-shaped branched DNA (X-DNA) was designed as TTP monomers, which consisted of four corresponding single-stranded DNA (ssDNA) (Um et al., 2006; Yang et al., 2018). Through rational sequence design, ssDNA was composed of intermolecular binding region (marked by black in Scheme 1A) for the construction of X-DNA and sticky ends (marked by red) for recognition with specific target DNA (transfer DNA [T-DNA]). Four ssDNA ($ssDNA_1$, $ssDNA_2$, $ssDNA_3$, and $ssDNA_4$) self-assembled to from X-DNA with optimized annealing procedure. In TTP system, two types of X-DNA (X_1 and X_2) were designed as monomers to further form DNA nanospheres. X_1 and X_2 had the same binding core and different sticky ends, which were complementary with specific T-DNA. Through this design, T-DNA functioned both as initiators to trigger

the polymerization of X-DNA and as linkers to hybridize with X_1 and X_2, consequently forming DNA nanospheres (Scheme 1B). It was notable that the formation of polymeric DNA nanospheres only occurred in the presence of T-DNA. In addition, the TTP system did not require any enzymes, reducing the operational complexity and potentially facilitating future applications such as point-of-care testing (POCT). Specifically, compared with other enzyme-free amplification methods, such as HCR (Tang et al., 2012) and strand displacement reaction (Li et al., 2015; Wang et al., 2012), the TTP system avoided the steps of toehold migration and hairpin structure de-conformation, which therefore enabled the formation of DNA nanospheres in a very short period of time. In other words, simultaneous recognition and amplification was achieved in a one-step reaction and in an enzyme-free and rapid manner.

We first constructed X-DNA by mixing four corresponding ssDNA at equimolar concentrations and with further annealing procedure. The successful synthesis of X-DNA was characterized and confirmed by gel electrophoresis (Figure S1A). The addition of T-DNA into the mixture of X_1 and X_2 initiated the polymerization of DNA nanospheres. Polymeric DNA nanospheres with higher molecular weights were observed in agarose gel electrophoresis (Figure S1B). The bands in gel hole indicated the successful synthesis of DNA nanospheres. A long-tail smear in the lanes of X_1+X_2+ T-DNA existed, which corresponded to the DNA nanospheres with broad size distribution. In contrast, in the absence of T-DNA or in the presence of background DNA (B-DNA), no band of DNA nanospheres was observed (in the lanes X_1+X_2+PBS and X_1+X_2+B-DNA in Figure S1B), indicating that polymerization did not occur. These results confirmed that T-DNA specifically triggered the polymerization of X-DNA into DNA nanospheres. The synthesized DNA nanospheres were also verified by atomic force microscopy imaging (Figure S1C). In addition, we explored the formation of DNA nanospheres over time. After the addition of T-DNA in the mixture of X_1 and X_2 for 2 min, the band in the gel hole with strong fluorescence intensity indicated that the formation of DNA nanospheres started within 2 min (Figure S2). Also, the fluorescence intensity of the smear became relatively lighter over time, suggesting that the dynamic assembly of DNA nanospheres continuously proceeded from 2 to 60 min.

Real-Time TTP System at Bio-interface for One-Step Signal Amplification

For real-time monitoring of the TTP-based process, we took advantage of the quartz crystal microbalance (QCM) as a signal output device. QCM has the ability to measure extremely small mass changes at the nanogram level by monitoring in real-time the frequency changes of quartz crystal resonator. QCM, therefore, has been developed as a label-free biosensor for the sensitive analysis of biomolecules and kinetic evaluation (Cheng et al., 2012; John et al., 2014).

The TTP-based system included two key stages: molecular recognition for T-DNA and signal amplification by TTP (Figure S3A). To efficiently recognize T-DNA, we designed capture DNA (C-DNA) probes for complementary pairing with T-DNA, which contained a thiol group for immobilizing on the chip surface by Au-S bond and a poly(A) tail for increasing the distance between the probes and chip surface and reducing the "size dilemma" (Lin et al., 2015). In addition, the chip with C-DNA attached was blocked by 6-mercapto-1-hexanol (MCH) to avoid non-specific adsorption. In TTP-based system, the immobilized C-DNA probes specifically hybridized with partial sequences of T-DNA, generating a corresponding molecular recognition signal. Afterward, the remaining single-strand region of T-DNA was exposed for subsequent signal amplification.

We first studied effective one-step signal amplification by the TTP system. We synthesized DNA nanospheres with X_1 in the periphery at a certain proportion of T-DNA and X-DNA, to allow their effective hybridization with T-DNA (Figure S3B). The frequency signals decreased slightly and then further decreased significantly after introducing T-DNA and DNA nanospheres with X_1 on the periphery, respectively (Figure S3C). Interestingly, we observed that the values of frequency changes (Δf) and rates ($d\Delta f/dt$) both changed in the process of signal amplification relative to target recognition, owing to the introduction of DNA nanospheres with high molecular weight. In contrast, the frequency signal remained unchanged when applying B-DNA and the following mixture of X_1 and X_2 (Figure S3C), confirming the high specificity of the TTP system.

Layer-by-Layer TTP System for Step-by-Step Signal Amplification

We further developed a layer-by-layer TTP system to regulate the self-assembly of DNA nanospheres that was *in situ* growing on QCM chip, achieving step-by-step signal amplification. In detail, after the incubation of C-DNA and MCH, the chip was capable of T-DNA-specific recognition and capture. After the addition of T-DNA, X_1 was introduced due to the complementary pairing between exposed sequences of T-DNA and

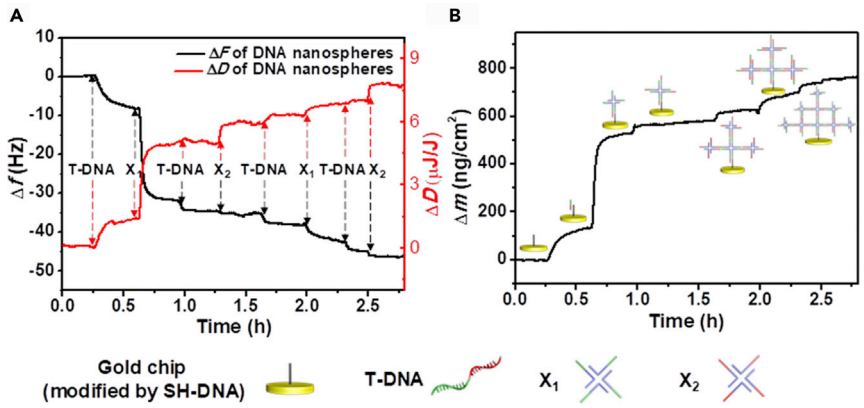

Figure 1. Real-Time Monitoring of Layer-by-Layer TTP System for Step-by-Step Signal Amplification

(A) Frequency and dissipation changes of the self-assembled DNA nanospheres in the TTP system. Stepped frequency and dissipation change signals clearly showed the feature of layer-by-layer TTP system to form DNA nanospheres via four cycles. In the first cycle, a dramatic change reflected the efficient hybridization, and the accumulated introduction of T-DNA and X-DNA obviously increased the signals.

(B) Corresponding Δm of the self-assembled DNA nanospheres in the TTP system calculated by Sauerbrey equation.

sticky end of X_1, followed by T-DNA and X_2. By the sequential injection of T-DNA and X-DNA as a cycle, layer-by-layer self-assembled DNA nanospheres were *in situ* assembled on chip surface after several cycles, and consequently, TTP systems realized effective step-by-step signal amplification. Finally, the frequency signals were used as real-time outputs to monitor the polymerization of DNA nanospheres, where Δf and $d\Delta f/dt$ reflected hybridization thermodynamic and kinetic behaviors, respectively. In addition, the chip was regenerated after treatment with denaturant for the next round of testing, demonstrating the reusability and cost-effectiveness (Figure S4).

To determine the optimal concentration ratio of T-DNA to X-DNA, we set three groups of experiments. We defined the differences in Δf values between final equilibrium states and baseline as ΔF. The Δf values decreased twice after the introduction of T-DNA and X-DNA, which were recorded as ΔF_1 and ΔF_2, respectively. Also, the values of $\Delta F_2/\Delta F_1$ reflected the hybridization capacity of X-DNA relative to T-DNA. By comparing the values of $\Delta F_2/\Delta F_1$, the concentration ratio of T-DNA: X-DNA at 2:1 had the highest hybridization capacity, which was used for subsequent experiments (Figure S5). After four cycles in layer-by-layer TTP system, Δf and dissipation change (ΔD) were clearly distinguished, demonstrating excellent capability of target recognition and signal amplification (Figure 1A). During the first cycle, the frequency response showed a slowly decreasing trend (from 0 Hz to −8 Hz) and then a dramatic decrease (from −8 to −31 Hz), owing to the effective hybridization between T-DNA and X_1. Next, the accumulated introduction of T-DNA and X-DNA contributed to a multistep drop (from −31 to −46 Hz). Although the decrease after the first cycle was relatively slight due to space resistance and electrostatic repulsion (Zhao et al., 2015b), our layer-by-layer TTP system significantly improved the sensitivity of biosensor. Meanwhile, the corresponding mass changes were calculated by Sauerbrey equation applied in aqueous solutions (Kanazawa and Gordon, 1985; Kanazawa and Ii, 1985)

$$\Delta f = -f_0^{3/2}\sqrt{\frac{n\rho_l\eta_l}{\pi\rho_q\mu_q}} = -C\Delta m$$

where f_0 is the resonance frequency of the bare resonator; n is the number of the overtone; ρ_l and η_l are the density and viscosity of liquid, respectively; ρ_q and η_q are the density and shear modulus of quartz, respectively; and C is a proportionality constant according to the intrinsic parameters of the QCM device. As a result there was a linear relationship between the change of mass (Δm) and Δf when the flexible conformation of branched DNA was ignored (Okahata et al., 1998; Vogt et al., 2004). A gradient of mass change curve indicated the growth of DNA nanospheres triggered by T-DNA (Figure 1B).

We further examined the sensitivity of layer-by-layer TTP system. The frequency signals were monitored in the range of T-DNA concentrations from 2 pM to 0.2 μM, presenting a gradual increasing trend. -ΔF and the

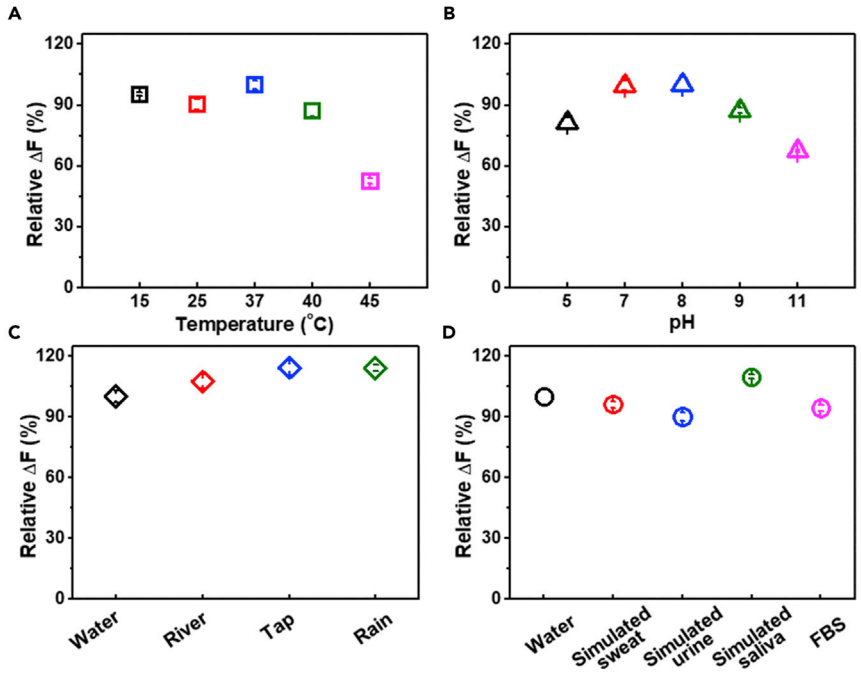

Figure 2. The TTP System Exhibited Excellent Robustness and Reliability in Relatively Harsh Environments

(A) The relative Δ*F* signals demonstrated the robustness of the TTP system under different temperatures (n = 3, mean ± SD).

(B) The relative Δ*F* signals demonstrated the robustness of the TTP system under different pH (n = 3, mean ± SD).

(C) The relative Δ*F* signals demonstrated the robustness of the TTP system under different water environments (n = 3, mean ± SD).

(D) The relative Δ*F* signals demonstrated the robustness of the TTP system under different simulated biological fluids (n = 3, mean ± SD).

logarithmic values of T-DNA concentrations showed linear relationships of y = 5.696x-25.195 (R^2 = 0.9286) and y = 8.511x-37.456 (R^2 = 0.9608) in the range of 20 pM to 20 nM, corresponding to one-cycle and three-cycle amplifications, respectively (Figure S6). Compared with the one-cycle curve, the slope of the Δ*F* curve corresponding to three cycles was improved by nearly 1.5 times, which contributes to the effective signal amplification. There existed two abnormal values: the point at 0.2 μM was mainly due to the complex nanostructures formed among individual DNA nanospheres, resulting in the enhanced frequency signal; the point at 2 pM was mainly due to the high background signal. As a result, the limit of detection was determined as 20 pM.

TTP System Had Excellent Robustness and Reliability over a Wide Range of Conditions

The aforementioned results demonstrated that the TTP system worked well in laboratory-based conditions. We further tested the robustness and stability of the TTP system in realistic conditions, including different temperature, pH, water quality, and simulated biological fluids (Figure 2). We first verified that the formation of DNA nanospheres was not affected in the temperature range of 4°C–45°C by gel electrophoresis (Figure S7A). We further tested the temperature stability (15°C–45°C) of the TTP system on QCM device. The relative Δ*F* showed only slight fluctuations within the temperature range of 15°C–40°C, indicating the temperature stability of the TTP system (Figure S7B and 2A). The signal became weaker at 45°C because of the instability of Au-S bonds at a higher temperature (Gao et al., 2018; Hu et al., 2018). A gradient of pH from 3.0 to 13.0 was tested. The formed DNA nanospheres maintained integrity in both weak acidic and weak basic buffers except for pH 3.0 (Figure S8A), which was mainly due to DNA degradation induced by protonation of adenine (A), guanine (G), and cytosine (C) under strong acid condition (Colotte et al., 2011; Huang et al., 2016). The frequency signals were detected distinctly in solutions with different pH from 5.0 to 11.0 (Figure S8B). In spite of the slight decrease in acidic buffers of pH 5.0 or in basic buffers of pH 11.0, the relative Δ*F* was sufficiently distinguishable for T-DNA detection (Figure 2B). We

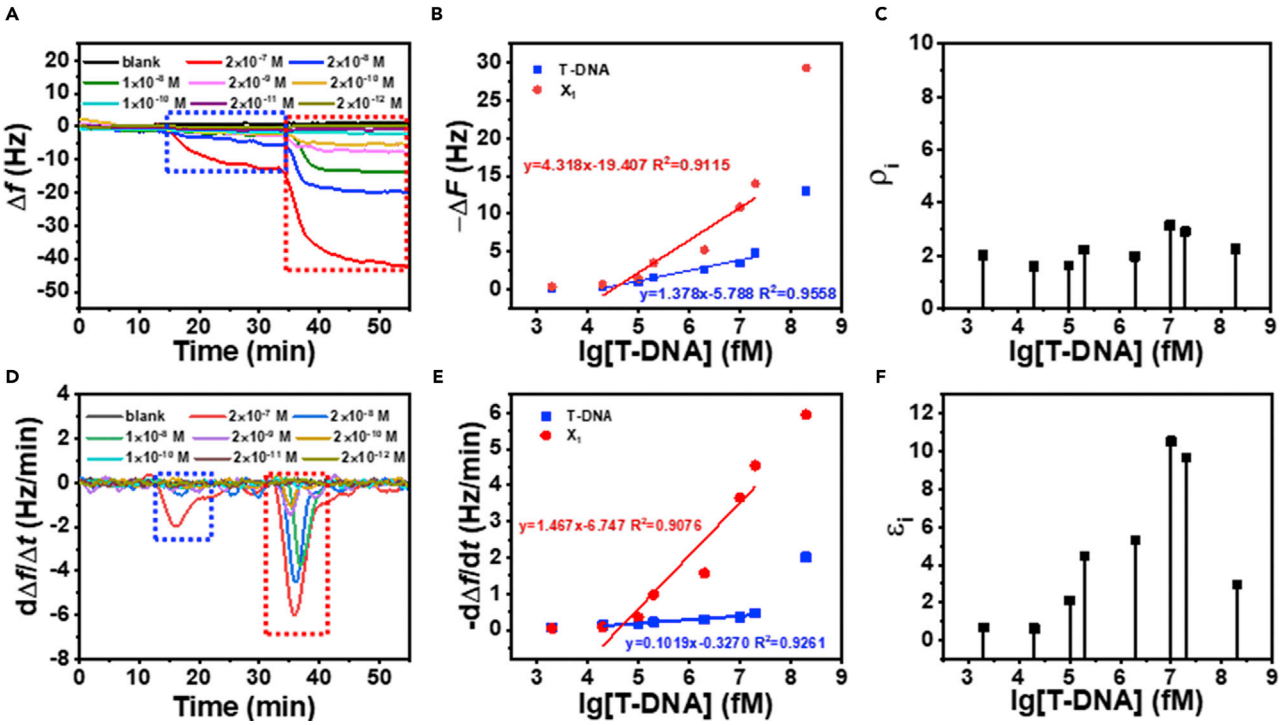

Figure 3. TTP System Showed Enhanced Hybridization Thermodynamic and Kinetic Performance

(A) The Δ*f* curves changing with time.

(B) The -Δ*F* curves after the introduction of T-DNA (marked with blue) and X_1 (marked with red) changing with T-DNA concentrations.

(C) ρ_i reflecting DNA hybridization thermodynamics, which remained constant within a concentration range of 2×10^{-7} to 2×10^{-12} M.

(D) The dΔf/d*t* curves changing with time, reflecting instantaneous hybridization rates of T-DNA with different concentrations.

(E) The -dΔf/d*t* curves after the introduction of T-DNA (marked with blue) and X_1 (marked with red) changing with T-DNA concentrations.

(F) ε_i increasing first and then decreasing within a concentration range of 2×10^{-7} to 2×10^{-12} M, which was limited by probe density and steric hindrance.

further tested the robustness of DNA nanospheres in various water qualities. DNA products formed in different environments (pure, reservoir, river, well, rain, and tap) showed obvious bands in gel holes (Figure S9), which indicated that the formation of DNA nanospheres was not affected by the water quality. The robust performance of TTP systems was also tested by QCM experiments. The obtained relative Δ*F* results clearly demonstrated that the TTP system performed reliably in a relatively wide range of non-laboratory water environments, such as pure, river, tap, and rain water (Figure 2C). Finally, to evaluate the clinical feasibility and future potentiality of TTP system, four simulated biological fluids as medium were used to assess the reliability of the TTP system, including simulated sweat, simulated urine, simulated saliva, and fetal bovine serum. It was confirmed by both gel electrophoresis and frequency curves on QCM that DNA nanospheres were extremely stable in various simulated biological fluids (Figure S10). The relative Δ*F* of simulated biological fluids had slight fluctuations in the range of ±20% (Figure 2D). According to these results, the TTP system demonstrated excellent robustness and reliability for T-DNA detection in relatively harsh conditions.

TTP System Exhibited Enhanced Hybridization Thermodynamics and Kinetics Performances at Different T-DNA Concentrations

In the aforementioned experiments, we observed that different T-DNA concentrations simultaneously influenced Δ*f* and dΔf/d*t*, which corresponded to hybridization thermodynamics and kinetics, respectively. We studied the thermodynamics and kinetics of DNA hybridization at the biosensing interface (Figure 3), by taking the first cycle of TTP system in Figure S6A as an example.

In terms of hybrid thermodynamics, the horizontals of frequency signal curves after the addition of T-DNA and X_1 (marked by blue and red, respectively) were set as the equilibrium states of two hybridization

reactions, which reflected the termination of hybridization thermodynamics (Figure 3A). As ΔF was linear with Δm, $-\Delta F_{i-T-DNA}$ or ΔF_{i-X1} after the introduction of T-DNA or X_1 represented the corresponding hybridization yields, where i was the concentration of T-DNA. The $-\Delta F$ gradually improved linearly within a T-DNA concentration range of 20 pM to 20 nM (Figure 3B) (Chen et al., 2013). The addition of T-DNA and X_1 corresponded to the linear curves of y = 1.378x-5.788 (R^2 = 0.9558) and y = 4.318x-19.407 (R^2 = 0.9115), respectively. To clearly understand the hybridization thermodynamics, we defined ρ_i as the hybridization capacity of X_1 to T-DNA at T-DNA concentrations of i.

$$\rho_i = \frac{\Delta m_{i-X1}}{\Delta m_{i-T\text{-}DNA}} = \frac{-\Delta F_{i-X_1}}{-\Delta F_{i-T\text{-}DNA}}$$

Figure 3C showed that ρ_i had a slight fluctuation around the value of 2, which indicated that the hybridization capacity remained almost unchanged within a range of T-DNA concentrations. According to the molecular weight and concentration ratio (2:1) of T-DNA and X_1, we calculated the theoretical ratio of hybridization yield (ρ_T) to be approximately 3.5.

$$\rho_T = \frac{MW\ (X_1)}{2 \times MW\ (T\text{-}DNA)}$$

On the basis of experimental and theoretical ratio of hybridization yield, we obtained hybridization efficiency (ω_i) at different T-DNA concentrations (Table S2), which reached an average level of 60% at the biosensing interface.

$$\omega_i = \frac{\rho_i}{\rho_T}$$

We analyzed the influencing factors for the hybridization efficiency between T-DNA and X-DNA in the following aspects: (1) the topologies of DNA on the chip were uncontrollable, such as the influence of non-specific adsorption (Pei et al., 2014); (2) the presence of spatial resistance restricted the effective binding of X-DNA and T-DNA (De Luna et al., 2017); (3) the high electron cloud density on chip surface caused electrostatic repulsion to hinder the binding of X-DNA; and (4) the X-DNA was washed away before binding at a certain flow rate. To sum up, hybridization efficiency could be further improved by overcoming these limitations.

In terms of hybridization kinetics, $d\Delta f/dt$ curves were drawn to display the instantaneous DNA hybridization rates at different T-DNA concentrations (van der Meulen et al., 2014), where two peaks (labeled by blue and red) appeared when the introduction of T-DNA and X-DNA, respectively (Figure 3D). We observed that the instantaneous hybridization rates reached a maximum shortly at the beginning of hybridization, and the polymerization lasted for a few minutes, reflecting the rapid performance of TTP system on the biosensing interface. To describe the kinetic characteristics of DNA hybridization, we plotted the instantaneous hybridization rates $-d\Delta f_{i-T-DNA}/dt$ and $-d\Delta f_{i-X1}/dt$ corresponding to T-DNA and X_1 as a function of T-DNA concentrations, where i represented the concentration of T-DNA (Figure 3E). The $-d\Delta f/dt$ curves varied linearly within the T-DNA concentration range (2×10^{-11}-2×10^{-8} M). The fitted curves were y = 0.1029x-0.3270 (R^2 = 0.9261) and y = 1.467x-6.747 (R^2 = 0.9076), corresponding to the addition of T-DNA and X_1. The slope of $-d\Delta f_{i-X1}/dt$ curve was increased by 14 times to that of the $-d\Delta f_{i-T-DNA}/dt$ curve, illustrating the significantly enhanced hybridization kinetics by the TTP system owing to the introduction of X-DNA with higher molecular weight. We then defined ε_i as the ratio of instantaneous hybridization rates to explore the concentration dependence of hybridization kinetics.

$$\varepsilon_i = \frac{-d\Delta f_{i-X_1}/dt}{-d\Delta f_{i-T\text{-}DNA}/dt}$$

In Figure 3F, the ε_i increased first with the increase of T-DNA concentration in the range of 2×10^{-12} to 1×10^{-7} M, reaching as high as 10, and began to decrease when the T-DNA concentration exceeded 10 nM, revealing an optimal kinetic concentration of 10 nM. Because hybridization kinetics were attributed to both mass transfer and effective collision, the ratio of hybridization rates was limited to effective collision at lower concentrations and to mass transfer at higher concentrations (Lin et al., 2015). When T-DNA was at a lower concentration, the amount of T-DNA used for X_1 conjugation was limited, so as to generate a lower collision efficiency. In contrast, when T-DNA was at a relatively higher concentration, T-DNA with higher density caused space crowding at biosensing interface, further obstructing effective mass diffusion and transfer. As a result, both the limited T-DNA number and the crowded space restricted the DNA hybridization, leading to the lower hybridization kinetics.

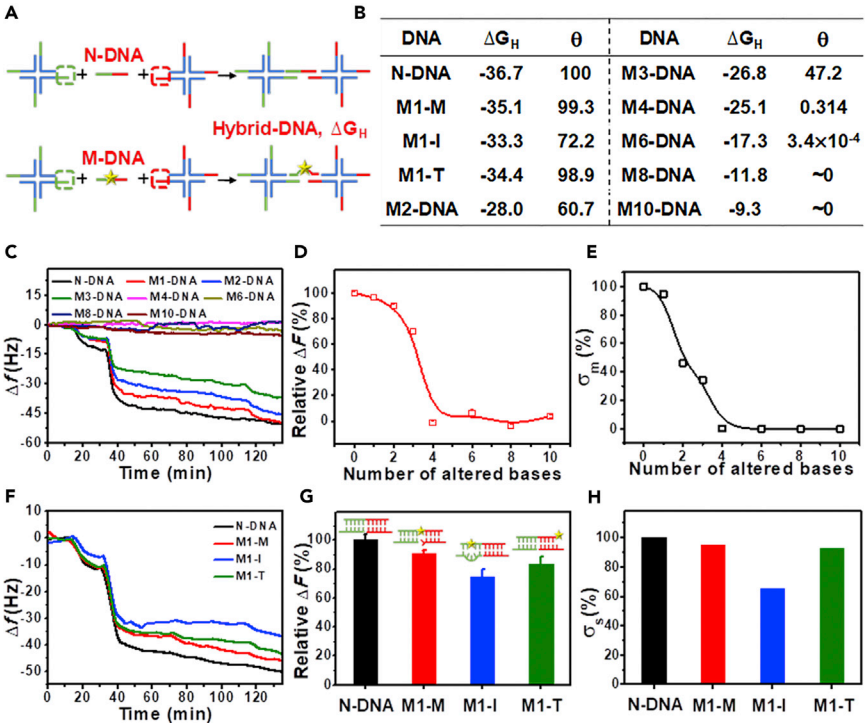

DNA	ΔG_H	θ	DNA	ΔG_H	θ
N-DNA	-36.7	100	M3-DNA	-26.8	47.2
M1-M	-35.1	99.3	M4-DNA	-25.1	0.314
M1-I	-33.3	72.2	M6-DNA	-17.3	3.4×10^{-4}
M1-T	-34.4	98.9	M8-DNA	-11.8	~0
M2-DNA	-28.0	60.7	M10-DNA	-9.3	~0

Figure 4. TTP System Achieved the Discrimination of Multi-base Changes and Single-Base Changes at Different Locations from Normal DNA

(A) The model of hybrid-DNA based on the hybridization process of N-DNA or M-DNA (non-complementary DNA with altered bases) with two types of X-DNA.

(B) The theoretical values of binding energy and equilibrium yields.

(C) The frequency curves of base-changing DNA with different number of altered bases.

(D) The relative ΔF of base-changing DNA with different number of altered bases (n = 3, mean ± SD).

(E) The theoretical σ_m of base-changing DNA with different number of altered bases. The experimental results were in good agreement with the theoretical analysis.

(F) The frequency curves of base-changing DNA with single-base changes at different positions.

(G) The relative ΔF of base-changing DNA with single-base changes at different positions (n = 3, mean ± SD).

(H) The theoretical σ_s of base-changing DNA with single-base changes at different positions. The experimental results were good agreement with the theoretical analysis.

From the above analysis, we observed that hybridization thermodynamics and kinetics exhibited different behaviors as a function of T-DNA concentration. Hybridization thermodynamics presented concentration independence, whereas hybridization kinetics depended on the T-DNA concentration owing to mass transfer and collision probability, proving guidance for the study of nucleic acid hybridization in interface chemistry.

TTP System Implemented Discrimination of Different Number of Base Changes and Positions of Single-Base Change

To investigate the selectivity and specificity of the TTP system, a series of DNA with non-complementary sequences (M-DNA) were introduced including single-base and multi-base changes relative to normal DNA (N-DNA) (Table S3). N-DNA functioned as linkers for binding two types of X-DNA to generate stable DNA nanospheres. However, metastable DNA nanospheres were produced when substituted bases existed in a sequence (asterisk indicated substituted bases). As the number of substituted bases increased, DNA nanospheres became more unstable owing to the occurrence of bulges or mismatched bubbles (Chen et al., 2013), which reflected in the gradually decreased ΔF signals (Figure 4C). There were clearly distinguishable signals of M-DNA with one to four altered bases compared with N-DNA. Once the number of altered bases reached 4 (including 4, 6, 8 and 10 altered bases), the frequency signals remained almost unchanged. The phenomenon of sharp reduction was obviously observed from the curve of relative ΔF

(Figure 4D), suggesting four altered bases as the critical value of frequency signals. As a result of the low binding energy, hybridization between M-DNA and branched DNA was difficult, showing unchanged frequency signals. In addition, the intermolecular tension caused by mismatched bases also affected the base pairing (Bustamante et al., 2003). Interestingly, when only N-DNA or M-DNA was introduced, there were insignificant differences in the ΔF signal of non-complementary sequences with altered bases of 1, 2, and 3; however, significant differences were observed after the introduction of X-DNA (Figure 4D). These results indicated that the introduction of X-DNA achieved effective signal amplification and that the TTP system had a capability for the discrimination of base-changing DNA from normal DNA.

Furthermore, we studied the ability of the TTP system to discriminate single-base changes at different sites in a stretch of DNA. To ensure that the frequency changes were only related to the locations of single-base changes, the single base was set with the same change from C to G at different locations, including M1-M (TG16, middle), M1-T (TG30, terminal), and M1-I (TG11, internal). These mismatched sequences with single-base changes at different positions were clearly distinguishable from each other according to frequency signals, in which ΔF ranked as M1-M > M1-T > M1-I (Figure 4F). The small differences produced by N-DNA or single-base M-DNA were amplified by the addition of X-DNA, indicating that TTP-based signal amplification obviously distinguished the positions of single-base changes. When altered base appeared at the location of 16 or 30, the mismatch occurred only at the terminal of hybridization chains, which did not affect the pairing of surrounding bases. However, for the altered base at the location of 11, intermolecular mismatch caused incomplete pairing of adjacent bases due to the inherent molecular tension, even though adjacent base pairs were fully complementary (Figure 4G). In addition, unexpected DNA secondary structures also influenced the hybridization binding affinity (Zhang et al., 2018). For example, the Gibbs free energy (ΔG) of M1-I was about −4 kcal/mol when forming stable hairpin secondary structure, whereas M1-M and M1-T were only −0.44 kcal/mol (calculated by www.nupack.org) (SantaLucia and Hicks, 2004). As a result, the relative ΔF of M1-I was much smaller than that of M1-M and M1-T (Figure 4G).

The relative ΔF of M-DNA reflected the hybridization thermodynamics, which had a close relationship with binding energy of DNA nanospheres (Wang et al., 2016; Zhang et al., 2012). We therefore systematically analyzed the theoretical binding energy of non-complementary sequences, including multi-base changes and single-base changes at different sites. To predict the hybridization situation of target DNA (including N-DNA and M-DNA) more effectively and reduce the complexity of algorithm, we reasonably simplified the DNA nanospheres into a theoretical model of hybrid-DNA nanostructures, as demonstrated in Figure 4A. We obtained the theoretical ΔG of hybrid-DNA nanostructures (ΔG_H) under the corresponding experimental conditions (Figure 4B, calculated by www.nupack.org; Dirks et al., 2007). The curve of relative ΔG_H varied with the number of altered bases (Figure S11), whose S-type trend was similar to the experimental results by and large. However, the appearance of several abnormal points with 4 and 6 altered bases indicated that the probability of the existence of hybrid-DNA was not only related to theoretical ΔG_H. We therefore introduced hybridization probability (σ) of single-base changes (σ_s) and multi-base changes (σ_m), which was affected by the combination of theoretical relative ΔG_H and corresponding equilibrium yields (θ_s and θ_m, described as θ):

$$\sigma = \Delta G_H \times \theta$$

where θ represented a fraction of equilibrium concentrations (calculated by www.nupack.org) of the expected structures to total concentrations.

$$\theta = \frac{\text{equilibrium concentrations}}{\text{total concentrations}}$$

In Figure 4B, θ_m values of M4-DNA and M6-DNA (0.314% and 0.00034%, respectively) were dramatically lower than those of the other sequences (M1-DNA, 99.3%; M2-DNA, 60.7%; M3-DNA, 47.2%), indicating that the content of hybrid-DNA constructed from M4-DNA and M6-DNA in solution was extremely low, which was another source of the abnormal points. As a result, ΔG_H and θ_m synergistically affected the probability of the existence of hybrid-DNA in solution. The resulting curve of σ_m had great agreement with the experimental results (Figure 4E). In terms of M-DNA with single-base changes at different sites, a similar phenomenon emerged. The theoretical ΔG_H was essentially consistent with the experimental frequency signals (Figure S12) except for the abnormal point of M1-I. The lower θ_s of M1-I (72.2%) relative to M1-M and M1-T was another primary cause of lower frequency signal. As a result, the σ_s values of M-DNA with single-base changes were in agreement with experimental values (Figure 4H), indicating the reliability of the theoretical model. Taking advantage of the established model, we predicted the hybridization

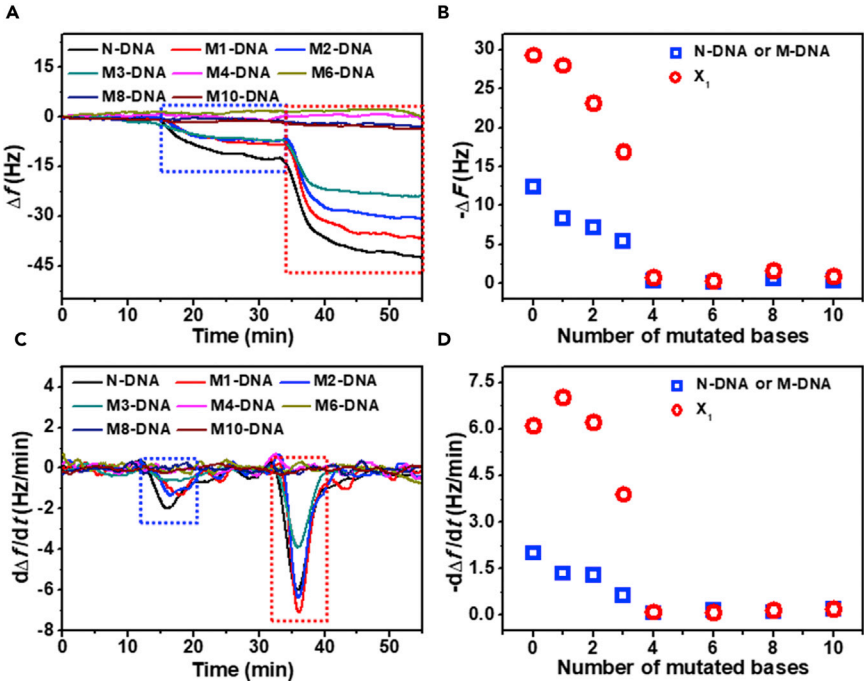

Figure 5. Improved Thermodynamic and Kinetic Performance by TTP System for the Discrimination of M-DNA and N-DNA

(A) The frequency curves of M-DNA and N-DNA changing with time.

(B) The $-\Delta F$ values after the introduction of T-DNA (marked with blue) and X_1 (marked with red) changing with the number of altered bases, reflecting hybridization efficiency with different number altered bases.

(C) The $d\Delta f/dt$ curves changing with time, reflecting instantaneous hybridization rates of M-DNA with different number of altered bases.

(D) The $-d\Delta f/dt$ values varying with the number of altered bases, reflecting the hybridization kinetics properties of M-DNA in TTP system.

probability of single-nucleotide change in long-strand DNA sequences (Table S4). With the increase of strand length, DNA sequences with single-base change tended to more occurrence of hybridization. The hybridization probability reached 99% when an altered base appeared in a stretch of 270-bp sequences, approaching the length limit of discrimination. In general, the abovementioned results showed that TTP system exhibited superior performances on the discrimination of altered DNA, including the number of altered bases (1–4 nt) and the positions of single-nucleotide changes. Moreover, TTP-based hybridization model effectively analyzed the hybridization probability of expected DNA nanostructures, which was influenced by both binding energy and equilibrium yield.

Improved Thermodynamics and Kinetics as the Fundamental Reason of Discriminating Base-Changing DNA

To explore the fundamental reason why base-changing DNA was effectively discriminated by the TTP system, we focused on the hybridization thermodynamics and kinetics in the first cycle of M-DNA and N-DNA in the TTP system (Figure 5A).

First, we studied the hybridization thermodynamics of M-DNA. As shown in Figure 5B, the $-\Delta F$ values after the addition of M-DNA or N-DNA and X_1 (marked by blue and red, respectively) reflected the corresponding hybridization yield, owing to the linearity between ΔF and Δm. We observed a dramatic decline on the $-\Delta F$ values of X_1 at the point of 4-base change; however, no dramatic change was observed on the $-\Delta F$ values of M-DNA or N-DNA. The phenomena indicated that the introduction of X_1 significantly increased the small differences of hybridization thermodynamics between M-DNA and N-DNA. According to the theoretical hybridization yield (ρ_T=3.5) calculated above, hybridization efficiencies (ω_i) of M-DNA and N-DNA were approximate 85%. Second, we analyzed the hybridization kinetics by plotting the $d\Delta f/dt$ curves of M-DNA and N-DNA with time and the $-d\Delta f/dt$ values with the number of altered bases (Figures 5C

and 5D). The ratio of the instantaneous hybridization rates of X_1 and N-DNA or M-DNA increased to approximately 5 times at altered bases less than 4, demonstrating that the TTP system amplified the small differences of hybridization kinetics performance between N-DNA and M-DNA in an identical reaction. The above analysis indicated that the differences of hybridization kinetics and thermodynamic properties are the fundamental reasons for M-DNA discrimination in the TTP system.

DISCUSSION

Single-base changes are associated with various biological and biomedical implications, such as genetic diseases, antibiotic resistance, and cancers; the distinction of single-base changes was, therefore, important for revealing biological mechanisms and exploring the methods for disease treatment. Current methods for distinguishing single-base changes mainly include PCR, sequencing technology, and hybridization (Khodakov et al., 2016). The traditional PCR and sequencing technology are mostly applied for distinguishing single-base changes; however, these methods have some intrinsic disadvantages, such as time consumption, high cost, complicated operation, low specificity, and so on. As a result, a large number of hybridization-based methods are developed for detecting base mutations, including protein-assistant hybridization, thermal denaturation-based hybridization, and direct hybridization (Knez et al., 2014). Protein-assistant hybridization needs to maintain enzyme activity during manipulating, and thermal denaturation-based hybridization needs the participation of precise temperature-control device, which undoubtedly increase the cost and difficulty of use. Relatively speaking, direct hybridization is the easiest way to operate. Our TTP system depended on the direct hybridization of nucleic acid, and there is no involvement of any enzyme and temperature control device, which made the operation very simple and low cost. The key to direct hybridization-based methods is the hybridization design. The common strategies are to design the constrained probes or to modify chemical molecules on hybridization probes (Abi and Safavi, 2019). Relative to some constrained probes (e.g., hairpin probes and strand displacement probes) and modified molecule (e.g., molecule beacons, artificial nucleic acid) probes, ssDNA as probes in our TTP system is the easiest and cheapest form. Moreover, the ssDNA probes and X-DNA amplifiers avoided the steps of toehold migration and structure de-conformation, enabling the rapid performance of the TTP system. In addition, the use of QCM biosensor provided convenience for detecting single-base changes with high specificity and selectivity, and for studying hybridization kinetics and thermodynamics of nucleic acid. As a whole, compared with the serious drawbacks in current methods, such as complicated operation, time-consumption, high cost, and low specificity, our TTP system possessed multiple unprecedented advantages including portable design, rapid manner, robust performance, enzyme-free amplification, label-free signal readout, and labor-free usage, fully satisfying the requirements of point-of-care testing.

In conclusion, we proposed a branched DNA-based TTP strategy for the enzyme-free and fast discrimination of base-changing DNA from normal DNA and developed a theoretical method for analyzing the hybridization probability of expected DNA structures. In TTP system, target DNA triggered the self-assembled polymerization of two species of X-DNA to construct DNA nanospheres, realizing rapid target recognition and signal amplification for picomolar-level DNA detection. The formation of DNA nanospheres only occurred in the presence of target DNA, without the involvement of any enzymes, ensuring the specificity and simplicity of the system. In addition, the TTP system exhibited excellent robustness and stability in a wide range of realistic conditions, including different pH and temperature, as well as a series of water sources and simulated biological fluids. Furthermore, we analyzed the hybridization thermodynamics and kinetics of the TTP system at different T-DNA concentrations: the hybridization kinetics depended on the T-DNA concentrations, whereas thermodynamics remains almost constant, providing insight for interface chemistry. Significantly, the TTP system had a powerful capability of discriminating not only the number of multi-base changes but also the positions of single-base changes. We proposed a theoretical model involving the synergistic effect of binding energy and equilibrium yields, based on which the hybridization probability of single-base and multi-base-changing DNA was analyzed and had a quite good correlation with the experimental results. We envision that our TTP system will be a powerful tool for the enzyme-free and fast discrimination of base-changing DNA in POCT and the theoretical analysis of nucleic acid hybridization.

Limitations of the Study

We implemented a new system for the discrimination of single-nucleotide changes. Although our TTP system exhibited excellent robustness and stability in a wide range of realistic conditions, as well as a series

of water sources and simulated biological fluids, our work had insufficient evidence in solving biological problems of relevance, such as testing of patient samples in real world. The limitation of this study will be taken into account in our near future researches.

METHODS

All methods can be found in the accompanying Transparent Methods supplemental file.

SUPPLEMENTAL INFORMATION

Supplemental Information can be found online at https://doi.org/10.1016/j.isci.2019.10.029.

ACKNOWLEDGMENTS

This work was supported in part by National Natural Science Foundation of China (grant no. 21621004, 21575101, 21622404, and 21704074), Ministry of Science and Technology of China (National Key Technology Research and Development Program, grant no.: 2018YFA0902302), Tianjin Natural Science Foundation (grant no.: 18JCJQJC47600), and Chinese Postdoctoral Science Foundation (2018M631735). We thank Dr. Zhikun Zhang at Hebei University of Science and Technology, Dr. Fusheng Pan at Tianjin University and Prof. Yang Liu at Nankai University for help on experiments. We thank Prof. Yongxi Zhao at Xi'an Jiaotong University for valuable suggestions.

AUTHOR CONTRIBUTIONS

Y.D. contributed to data curation, formal analysis, and writing of original draft. C.Y. contributed to formal analysis, writing of original draft, and funding acquisition. Z.W. contributed to the QCM measurements. D.L. contributed to revision of original draft. D.Y. contributed to revision of original draft, project administration, and funding acquisition.

DECLARATION OF INTERESTS

The authors declare no competing interests.

Received: June 28, 2019
Revised: September 24, 2019
Accepted: October 14, 2019
Published: November 22, 2019

REFERENCES

Abi, A., and Safavi, A. (2019). Targeted detection of single-nucleotide variations: progress and promise. ACS Sens. *4*, 792–807.

Ali, M.M., Li, F., Zhang, Z., Zhang, K., Kang, D.K., Ankrum, J.A., Le, X.C., and Zhao, W. (2014). Rolling circle amplification: a versatile tool for chemical biology, materials science and medicine. Chem. Soc. Rev. *43*, 3324–3341.

Bustamante, C., Bryant, Z., and Smith, S.B. (2003). Ten years of tension: single-molecule DNA mechanics. Nature *421*, 423–427.

Chen, S.X., Zhang, D.Y., and Seelig, G. (2013). Conditionally fluorescent molecular probes for detecting single base changes in double-stranded DNA. Nat. Chem. *5*, 782–789.

Chen, Y., Xu, J., Su, J., Xiang, Y., Yuan, R., and Chai, Y. (2012). In situ hybridization chain reaction amplification for universal and highly sensitive electrochemiluminescent detection of DNA. Anal. Chem. *84*, 7750–7755.

Cheng, C.I., Chang, Y.P., and Chu, Y.H. (2012). Biomolecular interactions and tools for their recognition: focus on the quartz crystal microbalance and its diverse surface chemistries and applications. Chem. Soc. Rev. *41*, 1947–1971.

Colotte, M., Coudy, D., Tuffet, S., and Bonnet, J. (2011). Adverse effect of air exposure on the stability of DNA stored at room temperature. Biopreserv. Biobank *9*, 47–50.

Cutler, J.I., Auyeung, E., and Mirkin, C.A. (2012). Spherical nucleic acids. J. Am. Chem. Soc. *134*, 1376–1391.

De Luna, P., Mahshid, S.S., Das, J., Luan, B.Q., Sargent, E.H., Kelley, S.O., and Zhou, R.H. (2017). High-curvature nanostructuring enhances probe display for biomolecular detection. Nano Lett. *17*, 1289–1295.

Dirks, R.M., Bois, J.S., Schaeffer, J.M., Winfree, E., and Pierce, N.A. (2007). Thermodynamic analysis of interacting nucleic acid strands. SIAM Rev. *49*, 65–88.

Gao, X.N., Jiang, L.L., Hu, B., Kong, F.P., Liu, X.J., Xu, K.H., and Tang, B. (2018). Au-Se-bond-based nanoprobe for imaging MMP-2 in tumor cells under a high-thiol environment. Anal. Chem. *90*, 4719–4724.

Gerasimova, Y.V., and Kolpashchikov, D.M. (2014). Enzyme-assisted target recycling (EATR) for nucleic acid detection. Chem. Soc. Rev. *43*, 6405–6438.

Greenman, C., Stephens, P., Smith, R., Dalgliesh, G.L., Hunter, C., Bignell, G., Davies, H., Teague, J., Butler, A., Stevens, C., et al. (2007). Patterns of somatic mutation in human cancer genomes. Nature *446*, 153–158.

Hu, B., Kong, F.P., Gao, X.N., Jiang, L.L., Li, X.F., Gao, W., Xu, K.H., and Tang, B. (2018). Avoiding thiol compound interference: a nanoplatform based on high-fidelity Au-Se bonds for biological applications. Angew. Chem. Int. Ed. *57*, 5306–5309.

Hu, S., Tang, W., Zhao, Y., Li, N., and Liu, F. (2017). Ultra-specific discrimination of single-nucleotide mutations using sequestration-assisted molecular beacons. Chem. Sci. *8*, 1021–1026.

Huang, J., Wu, Y., Chen, Y., Zhu, Z., Yang, X., Yang, C.J., Wang, K., and Tan, W. (2011). Pyrene-excimer probes based on the hybridization chain reaction for the detection of nucleic acids in

complex biological fluids. Angew. Chem. Int. Ed. *50*, 401–404.

Huang, R., He, N., and Li, Z. (2018). Recent progresses in DNA nanostructure-based biosensors for detection of tumor markers. Biosens. Bioelectron. *109*, 27–34.

Huang, Z., Liu, B., and Liu, J. (2016). Parallel polyadenine duplex formation at low pH facilitates DNA conjugation onto gold nanoparticles. Langmuir *32*, 11986–11992.

John, J., Hugar, K.M., Rivera-Melendez, J., Kostalik, H.A., Rus, E.D., Wang, H.S., Coates, G.W., and Abruna, H.D. (2014). An electrochemical quartz crystal microbalance study of a prospective alkaline anion exchange membrane material for fuel cells: anion exchange dynamics and membrane swelling. J. Am. Chem. Soc. *136*, 5309–5322.

Kanazawa, K.K., and Gordon, J.G. (1985). Frequency of a quartz microbalance in contact with liquid. Anal. Chem. *57*, 1770–1771.

Kanazawa, K.K., and Ii, J.G.G. (1985). The oscillation frequency of a quartz resonator in contact with a liquid. Anal. Chim. Acta *175*, 99–105.

Khodakov, D., Wang, C., and Zhang, D.Y. (2016). Diagnostics based on nucleic acid sequence variant profiling: PCR, hybridization, and NGS approaches. Adv. Drug Deliv. Rev. *105*, 3–19.

Knez, K., Spasic, D., Janssen, K.P., and Lammertyn, J. (2014). Emerging technologies for hybridization based single nucleotide polymorphism detection. Analyst *139*, 353–370.

Lahiry, P., Torkamani, A., Schork, N.J., and Hegele, R.A. (2010). Kinase mutations in human disease: interpreting genotype-phenotype relationships. Nat. Rev. Genet. *11*, 60–74.

Li, F., Dong, Y.H., Zhang, Z.K., Lv, M., Wang, Z., Ruan, X.H., and Yang, D.Y. (2018). A recyclable biointerface based on cross-linked branched DNA nanostructures for ultrasensitive nucleic acid detection. Biosens. Bioelectron. *117*, 562–566.

Li, H., Xiao, S., Yao, D., Lam, M.H., and Liang, H. (2015). A smart DNA-gold nanoparticle probe for detecting single-base changes on the platform of a quartz crystal microbalance. Chem. Commun. (Camb.) *51*, 4670–4673.

Lin, M., Wang, J., Zhou, G., Wang, J., Wu, N., Lu, J., Gao, J., Chen, X., Shi, J., Zuo, X., et al. (2015). Programmable engineering of a biosensing interface with tetrahedral DNA nanostructures for ultrasensitive DNA detection. Angew. Chem. Int. Ed. *54*, 2151–2155.

Liu, Q., Ge, Z., Mao, X., Zhou, G., Zuo, X., Shen, J., Shi, J., Li, J., Wang, L., Chen, X., et al. (2018). Valency-controlled framework nucleic acid signal amplifiers. Angew. Chem. Int. Ed. *57*, 7131–7135.

Niemz, A., Ferguson, T.M., and Boyle, D.S. (2011). Point-of-care nucleic acid testing for infectious diseases. Trends Biotechnol. *29*, 240–250.

Okahata, Y., Kawase, M., Niikura, K., Ohtake, F., Furusawa, H., and Ebara, Y. (1998). Kinetic measurements of DNA hybridisation an an oligonucleotide-immobilized 27-MHz quartz crystal microbalance. Anal. Chem. *70*, 1288–1296.

Pei, H., Lu, N., Wen, Y., Song, S., Liu, Y., Yan, H., and Fan, C. (2010). A DNA nanostructure-based biomolecular probe carrier platform for electrochemical biosensing. Adv. Mater. *22*, 4754–4758.

Pei, H., Zuo, X.L., Zhu, D., Huang, Q., and Fan, C.H. (2014). Functional DNA nanostructures for theranostic applications. Acc. Chem. Res. *47*, 550–559.

Rouge, J.L., Sita, T.L., Hao, L., Kouri, F.M., Briley, W.E., Stegh, A.H., and Mirkin, C.A. (2015). Ribozyme-spherical nucleic acids. J. Am. Chem. Soc. *137*, 10528–10531.

Sachidanandam, R., Weissman, D., Schmidt, S.C., Kakol, J.M., Stein, L.D., Marth, G., Sherry, S., Mullikin, J.C., Mortimore, B.J., Willey, D.L., et al. (2001). A map of human genome sequence variation containing 1.42 million single nucleotide polymorphisms. Nature *409*, 928–933.

SantaLucia, J., Jr., and Hicks, D. (2004). The thermodynamics of DNA structural motifs. Annu. Rev. Biophys. Biomol. Struct. *33*, 415–440.

Sauna, Z.E., and Kimchi-Sarfaty, C. (2011). Understanding the contribution of synonymous mutations to human disease. Nat. Rev. Genet. *12*, 683–691.

Schwarzenbach, H., Hoon, D.S.B., and Pantel, K. (2011). Cell-free nucleic acids as biomarkers in cancer patients. Nat. Rev. Cancer *11*, 426–437.

Smith, S.J., Nemr, C.R., and Kelley, S.O. (2017). Chemistry-driven approaches for ultrasensitive nucleic acid detection. J. Am. Chem. Soc. *139*, 1020–1028.

Tang, W., Wang, D., Xu, Y., Li, N., and Liu, F. (2012). A self-assembled DNA nanostructure-amplified quartz crystal microbalance with dissipation biosensing platform for nucleic acids. Chem. Commun. (Camb.) *48*, 6678–6680.

Um, S.H., Lee, J.B., Park, N., Kwon, S.Y., Umbach, C.C., and Luo, D. (2006). Enzyme-catalysed assembly of DNA hydrogel. Nat. Mater. *5*, 797–801.

van der Meulen, S.A., Dubacheva, G.V., Dogterom, M., Richter, R.P., and Leunissen, M.E. (2014). Quartz crystal microbalance with dissipation monitoring and spectroscopic ellipsometry measurements of the phospholipid bilayer anchoring stability and kinetics of hydrophobically modified DNA oligonucleotides. Langmuir *30*, 6525–6533.

Vogt, B.D., Lin, E.K., Wu, W.L., and White, C.C. (2004). Effect of film thickness on the validity of the Sauerbrey equation for hydrated polyelectrolyte films. J. Phys. Chem. B *108*, 12685–12690.

Wang, C., Bae, J.H., and Zhang, D.Y. (2016). Native characterization of nucleic acid motif thermodynamics via non-covalent catalysis. Nat. Commun. *7*, 10319.

Wang, D., Tang, W., Wu, X., Wang, X., Chen, G., Chen, Q., Li, N., and Liu, F. (2012). Highly selective detection of single-nucleotide polymorphisms using a quartz crystal microbalance biosensor based on the toehold-mediated strand displacement reaction. Anal. Chem. *84*, 7008–7014.

Xu, G.L., Zhoa, H., Reboud, J., and Cooper, J.M. (2018). Cycling of rational hybridization chain reaction to enable enzyme-free DNA-based clinical diagnosis. ACS Nano *12*, 7213–7219.

Yang, L., Yao, C., Li, F., Dong, Y.H., Zhang, Z.K., and Yang, D.Y. (2018). Synthesis of branched DNA scaffolded super-nanoclusters with enhanced antibacterial performance. Small *14*, e1800185.

Zhang, D.Y., Chen, S.X., and Yin, P. (2012). Optimizing the specificity of nucleic acid hybridization. Nat. Chem. *4*, 208–214.

Zhang, J.X., Fang, J.Z., Duan, W., Wu, L.R., Zhang, A.W., Dalchau, N., Yordanov, B., Petersen, R., Phillips, A., and Zhang, D.Y. (2018). Predicting DNA hybridization kinetics from sequence. Nat. Chem. *10*, 91–98.

Zhao, Y., Chen, F., Li, Q., Wang, L., and Fan, C. (2015a). Isothermal amplification of nucleic acids. Chem. Rev. *115*, 12491–12545.

Zhao, Y., Wang, H., Tang, W., Hu, S., Li, N., and Liu, F. (2015b). An in situ assembly of a DNA-streptavidin dendrimer nanostructure: a new amplified quartz crystal microbalance platform for nucleic acid sensing. Chem. Commun. (Camb.) *51*, 10660–10663.

Zhou, H., Liu, J., Xu, J.J., Zhang, S.S., and Chen, H.Y. (2018). Optical nano-biosensing interface via nucleic acid amplification strategy: construction and application. Chem. Soc. Rev. *47*, 1996–2019.

ISCI, Volume *21*

Supplemental Information

Target-Triggered Polymerization of Branched DNA Enables Enzyme-free and Fast Discrimination of Single-Base Changes

Yuhang Dong, Chi Yao, Zhi Wang, Dan Luo, and Dayong Yang

Supplemental Information

Supplemental figures and legends

Characterization of self-assembled DNA nanospheres

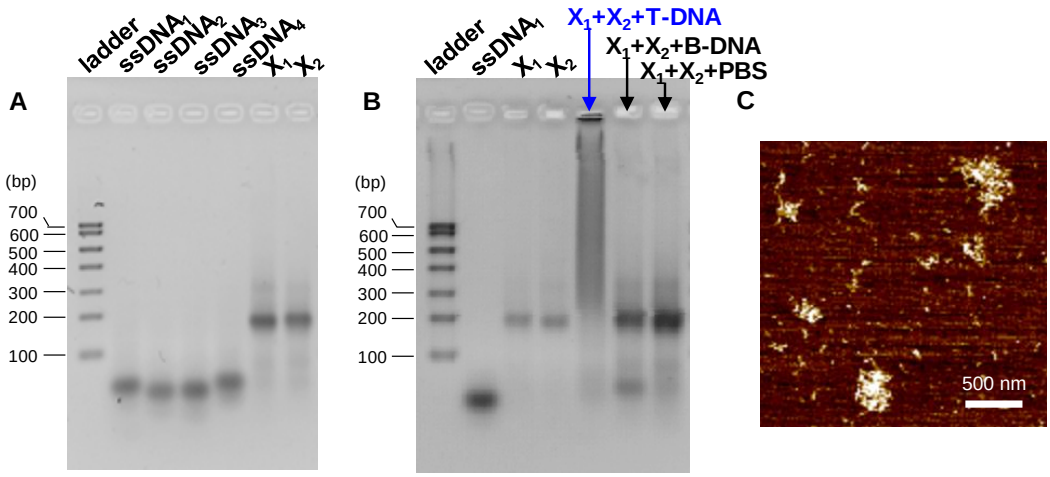

Figure S1. Characterization of self-assembled DNA nanospheres (related to Figure 1). Agarose gel electrophoresis (3%) were used to characterize the successful synthesis of (A) X-shaped DNA and (B) DNA nanospheres. The formation of DNA nanospheres only occurred in the presence of target DNA (T-DNA), and no DNA nanospheres was formed in the presence of background DNA (B-DNA) or in the absence of T-DNA. (C) Verification of the formation of DNA nanospheres by atomic force microscope (AFM).

Reaction time on the formation of DNA nanospheres

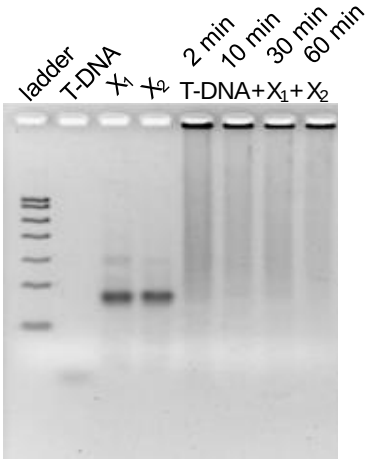

Figure S2. Effect of reaction time on formation of DNA nanospheres in TTP system by agarose gel electrophoresis (3%), indicating the rapid performance of TTP system (related to Figure 1).

Real-time TTP system for one-step signal amplification.

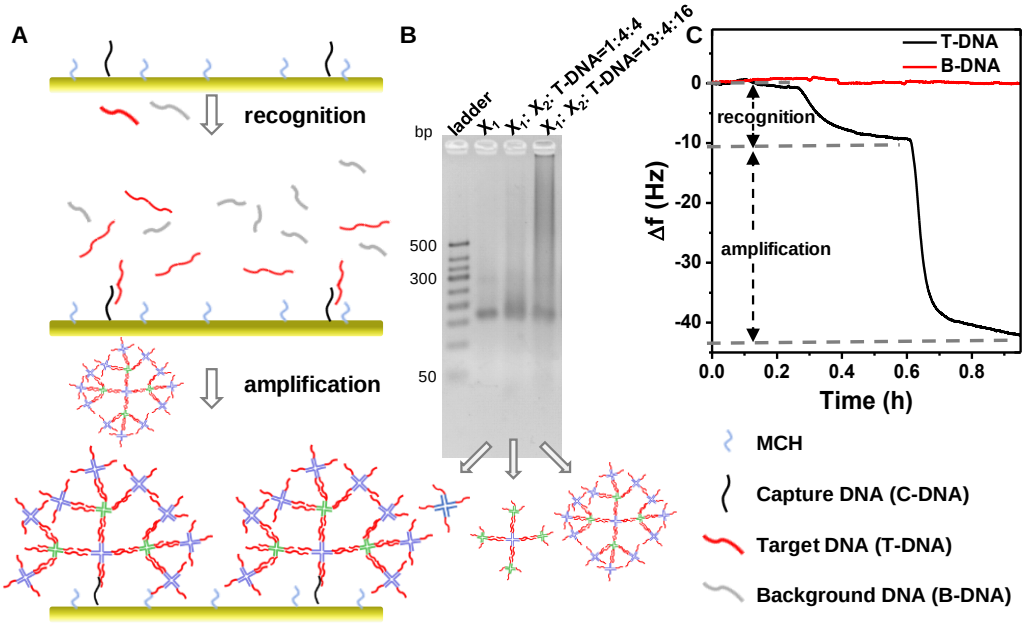

Figure S3. **Real-time TTP system for one-step signal amplification (related to Figure 1).** (A) Schematic diagram of real-time monitoring of target recognition and signal amplification by quartz crystal microbalance (QCM). (B) Agarose gel electrophoresis (3%) of DNA nanospheres with different hierarchy structures by the self-assembly of T-DNA and X-DNA, used to verify the successful formation of three-layered DNA nanospheres. (C) The reduction of frequency changes (black line) indicating target recognition between target DNA (T-DNA) with capture DNA (C-DNA), and signal amplification after the introduction of X-shaped DNA (X-DNA). In contrast, unchanged frequency signal remained in the presence of background DNA (B-DNA) (red line), exhibiting the specificity of TTP system.

Layer-by-layer TTP system for step-by-step signal amplification.

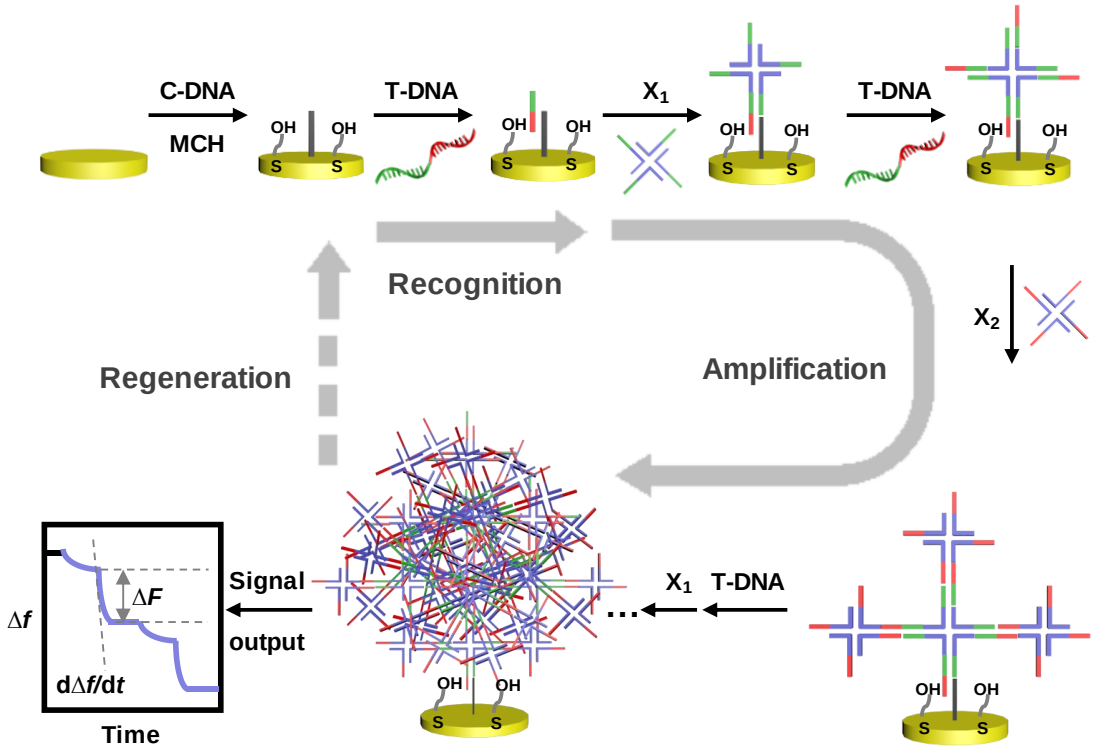

Figure S4. **Schematic illustration of layer-by-layer self-assembled DNA nanospheres *in situ* growth on a QCM chip, including the process of target recognition, step-by-step signal amplification and regeneration (related to Figure 1).** After the incubation of C-DNA and MCH, the chip recognized specific T-DNA. By the alternate introduction of T-DNA and X-DNA, layer-by-layer DNA nanospheres were constructed on the chip surface based on TTP system, realizing target recognition and step-by-step signal amplification. The frequency signal was used as the real-time output to monitor the growth of DNA nanospheres, where Δf and $d\Delta f/dt$ reflected the thermodynamics and kinetics behaviors of DNA hybridization, respectively.

Optimized proportion of T-DNA to X-DNA

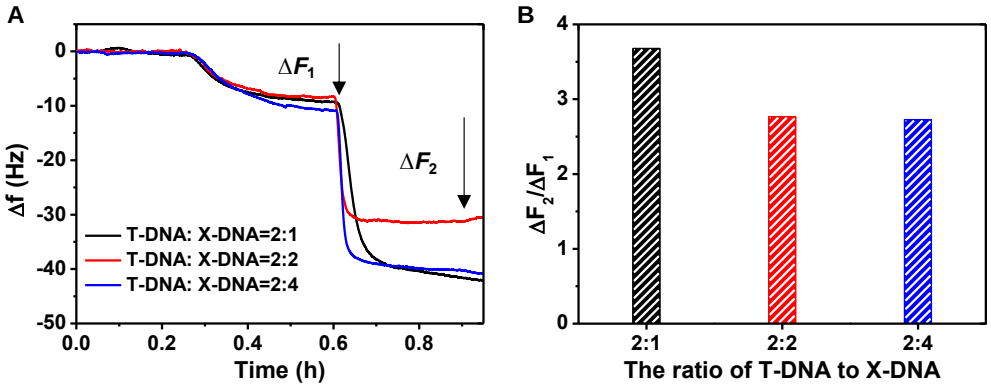

Figure S5. The optimization concentration ratio of T-DNA to X-DNA (related to Figure 1). (A) Frequency signal curves. (B) Statistics of $\Delta F_2/\Delta F_1$ upon a series of T-DNA/X-DNA ratios.

The sensitivity of layer-by-layer TTP system

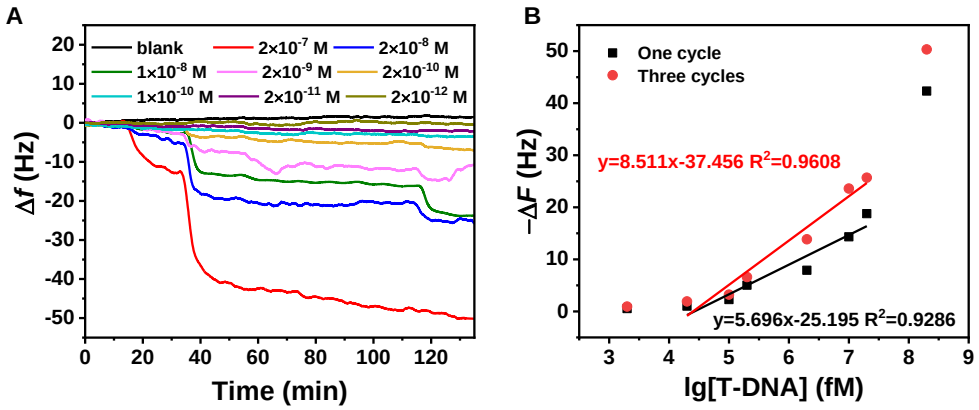

Figure S6. Sensitivity of DNA detection based on TTP system (related to Figure 1). (A) Frequency curves of the detection of T-DNA from 0.2 μM to 2 pM after three cycles of amplification. (B) -Δ*F* as a function of T-DNA concentrations *via* one cycle (black) and three cycles (red), showing good linear relationships in the range of 20 pM to 20 nM.

Robustness tests of TTP

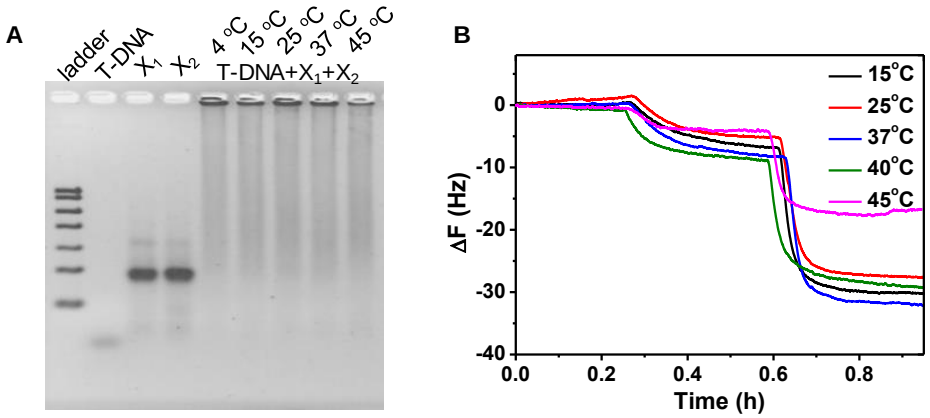

Figure S7. **The temperature stability of TTP system (related to Figure 2).** (A) Agarose gel electrophoresis (3%) used to verify the temperature stability of DNA nanospheres. (B) Frequency signal curves used to verify the temperature stability of TTP system on QCM.

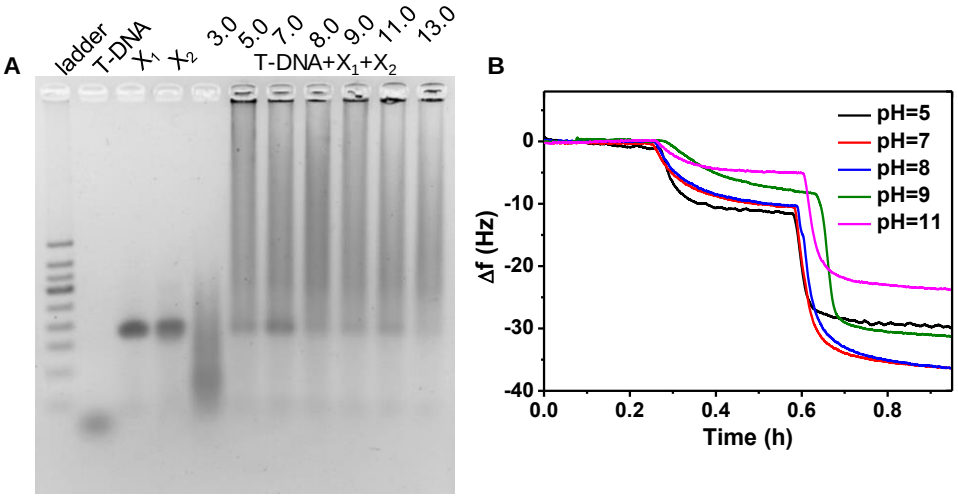

Figure S8. **The pH stability of TTP system (related to Figure 2).** (A) Agarose gel electrophoresis (3%) used to verify the pH stability of DNA nanospheres. (B) Frequency signal curves used to verify the pH stability of TTP system on QCM.

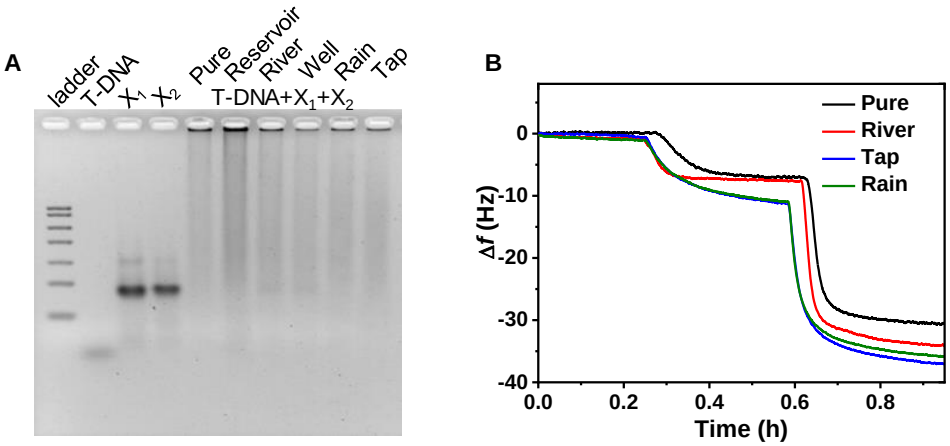

Figure S9. **The water environments stability of TTP system (related to Figure 2).** (A) Agarose gel electrophoresis (3%) used to verify the stability of DNA nanospheres in complicated water environments, such as reservoir, river, well, rain and tap. (B) Frequency signal curves used to verify the stability of TTP system on QCM in complicated water environments, such as river, tap and rain.

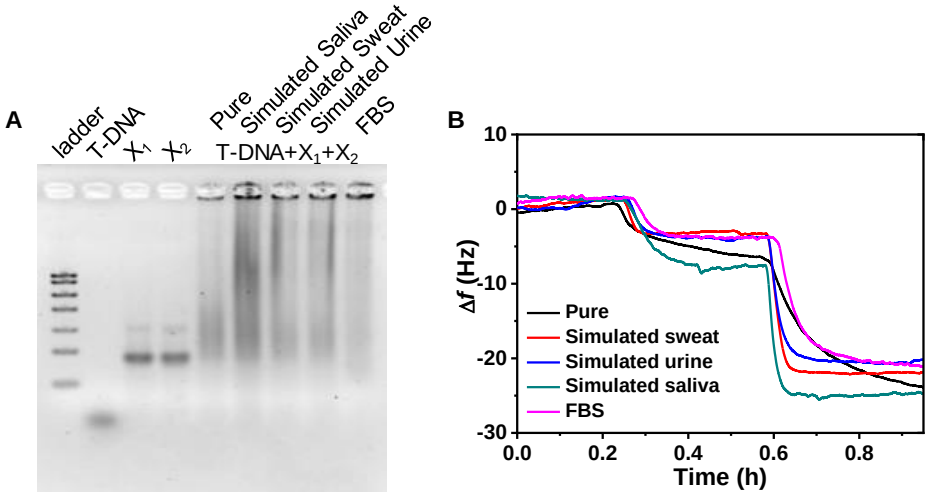

Figure S10. **The simulated body fluids stability of TTP system (related to Figure 2).** (A) Agarose gel electrophoresis (3%) used to verify the stability of DNA nanospheres in complex simulated body fluids including simulated sweat, simulated urine and simulated saliva, and fetal bovine serum (FBS). (B) Frequency signal curves used to verify the stability of TTP system on QCM in complex simulated body fluids and fetal bovine serum (FBS).

Theoretical analysis of hybrid-DNA

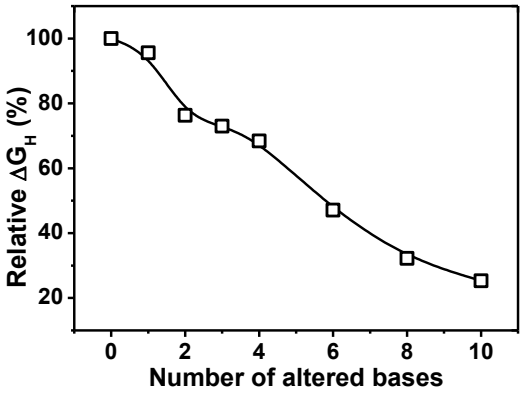

Figure S11. **The theoretical relative ΔG_H curves of hybrid-DNA with different number of altered bases (related to Figure 4).**

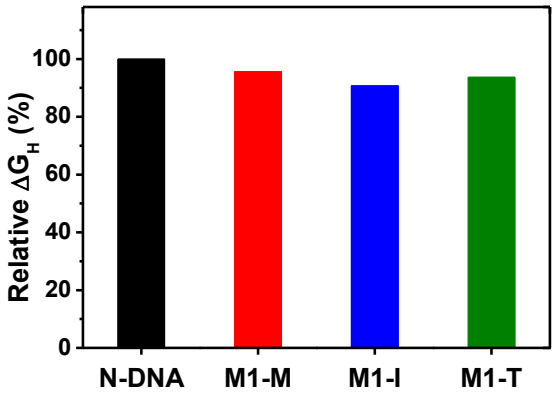

Figure S12. The theoretical relative ΔG_H values of hybrid-DNA with single-base changes at different positions (related to Figure 4).

Supplemental tables

Table S1. DNA sequences involved in enzyme-free TTP (related to Figure 1).

Strand	Sequence[a]	Use
Capture DNA (C-DNA)	5'HSAAAAAAAAAAGCCAATGTTCAGATG3'	Immobilization on the chip for capturing specific DNA
Normal DNA (N-DNA)	5'TCTTCATTCACAAAACATCTGAACATTGGC3'	Normal DNA as a linker for polymerization in TTP system.
$ssDNA_1$	5'TTTTGTGAATGAAGAGCTCATCCATGCCTAGACTGGCGATAAGTAGCCAGC3'	Oligonucleotides for the synthesis of X_1 and providing sticky end for the hybridization with target DNA.
$ssDNA_2$	5'TTTTGTGAATGAAGAGCTCAGCAAGCGTTATGCGTCTAGGCATGGATGAGC3'	
$ssDNA_3$	5'TTTTGTGAATGAAGAGCTCTGGTATGCATGTCGGCATAACGCTTGCTGAGC3'	
$ssDNA_4$	5'TTTTGTGAATGAAGAGCTGGCTACTTATCGCCACGACATGCATACCAGAGC3'	
$ssDNA_5$	5'CGACCGATGAATAGCGGTCAGATCCGTACCTACTCGGCCAATGTTCAGATG3'	Oligonucleotides for the synthesis of X_2 and providing sticky end for the hybridization with target DNA.
$ssDNA_6$	5'CGAGTAGGTACGGATCTGCGTATTGCGAACGACTCGGCCAATGTTCAGATG3'	
$ssDNA_7$	5'CGAGTCGTTCGCAATACGGCTGTACGTATGGTCTCGGCCAATGTTCAGATG3'	
$ssDNA_8$	5'CGAGACCATACGTACAGCACCGCTATTCATCGGTCGGCCAATGTTCAGATG3'	
Background DNA (B-DNA)	5'AAAGAGACCATCAATGAGGCAGAATGGGATAGATTG3'	Non-relevant DNA versus to target DNA.

[a]Complementary DNA sequences were represented by the same color.

Table S2. The hybridization efficiency at different DNA concentrations in TTP system (related to Figure 3).

T-DNA concentration (i)	Hybridization capacity (ρ_i)	Hybridization efficiency (ω_i)
2×10^{-7} M	2.0	57.1%
2×10^{-8} M	1.6	45.7%
1×10^{-8} M	1.6	45.7%
2×10^{-9} M	2.2	62.9%
2×10^{-10} M	2.0	57.1%
1×10^{-10} M	3.1	88.6%
2×10^{-11} M	2.9	82.9%
2×10^{-12} M	2.2	62.9%

Table S3. DNA sequences of non-complementary DNA with different number or positions of mismatched bases (related to Figure 4).

Strand	Sequence[a]	Use
M1-T	5’TCTTCATTCACAAAACATCTGAACATTGGG3’	Oligonucleotides with different number or positions of altered base sites versus to normal DNA (N-DNA) for exploring the specificity of detection system.
M1-I	5’TCTTCATTCAGAAAACATCTGAACATTGGC3’	
M1-M	5’TCTTCATTCACAAAAGATCTGAACATTGGC3’	
M2-DNA	5’TCTTCATTCAGAAAACATCTCAACATTGGC3’	
M3-DNA	5’TCTTCATTGACAAAAGATCTGACCATTGGC3’	
M4-DNA	5’TCTTCTTTCACATAACATGTGAACTTTGGC3’	
M6-DNA	5’TCTACATACACTAAACTTCTGTACATAGGC3’	
M8-DNA	5’TCATCAATCAGAAATCATGTGTACTTTCGC3’	
M10-DNA	5’TCATCCTTGAGAGAAGATCCGACCACTAGC3’	

[a]The altered base sites were marked in red.

Table S4. The hybridization probability prediction of single nucleotide changes in long stretch of DNA sequences by advantage of the established model (related to Figure 4).

Strand	Sequence[a]	ΔG_H (kcal/mol)	θ	σ
90 bp M1-I	5'TCTTCATTCACAAAACATCTGAACATTGGCTCTTCATTCAGAAAACATCTGAACATTGGCTCTTCATTCACAAAACATCTGAACATTGGC3'	-111.2	100%	97.1%
90 bp N-DNA	5'TCTTCATTCACAAAACATCTGAACATTGGCTCTTCATTCACAAAACATCTGAACATTGGCTCTTCATTCACAAAACATCTGAACATTGGC3'	-114.5	100%	100%
180 bp M1-I	5'TCTTCATTCACAAAACATCTGAACATTGGCTCTTCATTCACAAAATCTTCATTCACAAAACATCTGAACATTGGCTCTTCATTCAGAAAACATCTGAACATTGGCTCTTCATTCACAAAACATCTGAACATTGGCCATCTGAACATTGGCTCTTCATTCACAAAACATCTGAACATTGGC3'	-227.9	100%	98.5%
180 bp N-DNA	5'TCTTCATTCACAAAACATCTGAACATTGGCTCTTCATTCACAAAATCTTCATTCACAAAACATCTGAACATTGGCTCTTCATTCACAAAACATCTGAACATTGGCTCTTCATTCACAAAACATCTGAACATTGGCCATCTGAACATTGGCTCTTCATTCACAAAACATCTGAACATTGGC3'	-231.3	100%	100%
270 bp M1-I	5'TCTTCATTCACAAAACATCTGAACATTGGCTCTTCATTCACAAAACATCTGAACATTGGCTCTTCATTCACAAAACATCTGAACATTGGCTCTTCATTCAGAAAACATCTGAACATTGGCTCTTCATTCACAAAACATCTGAACATTGGCTCTTCATTCACAAAACATCTGAACATTGGCTCTTCATTCACAAAACATCTGAACATTGGC3'	-344.8	100%	99.0%
270 bp	5'TCTTCATTCACAAAACATCTGAACATTGGCTCTT	-348.2	100%	100%

N-DNA	CATTCACAAAACATCTGAACATTGGCTCTTCATTC
	ACAAAACATCTGAACATTGGCTCTTCATTCACAA
	AACATCTGAACATTGGCTCTTCATTCACAAAACAT
	CTGAACATTGGCTCTTCATTCACAAAACATCTGAA
	CATTGGCTCTTCATTCACAAAACATCTGAACATTG
	GCTCTTCATTCACAAAACATCTGAACATTGGCTCT
	TCATTCACAAAACATCTGAACATTGGC3’

[a]The altered base sites were marked in red.

Transparent methods

Chemicals and materials

All oligonucleotide sequences were purchased from Genewiz Biotech (Jiangsu, China). 6-Mercapto-1-hexanol (MCH) was purchased from Heowns (Tianjin, China) and Tris (2-carboxyethyl) phosphine hydrochloride (TCEP) was purchased from Qiming (Shanghai, China). DNA extraction reagent (Enol: Chloroform=25:24) was obtained from Solarbio (Beijing, China). Fetal bovine serum (FBS) was obtained from Zhejiang Tianhang Biotechnology Co., ltd. The main components of simulated saliva included 0.72 g/L KCl, 0.22 g/L $CaCl_2 \cdot H_2O$, 0.6 g/L NaCl, 0.68 g/L KH_2PO_4, 0.866 g/L $Na_2HPO_4 \cdot 12H_2O$, 1.5 g/L K_2CO_3, 0.06 g/L KSCN and 0.03 g/L citric acid. The main components of simulated sweat included 0.1% sodium chloride (NaCl), 0.1% lactic acid and 0.1% urea (% in mass) (Marques et al., 2011). The main components of simulated urine included 25.0 g/L urea, 9.0 g/L NaCl, 3.0 g/L NH_4Cl, 2.0 g/L creatinine, 2.5 g/L Na_2HPO_4, 2.5 g/L KH_2PO_4, 3.0 g/L, Na_2SO_3 (Liu et al., 2015). These simulated biological fluids were adjusted to pH 8. The 1×TE hybridization buffer was composed of 10 mM Tris, 1 mM EDTA·Na_2 and 0.1 M NaCl, and then be adjusted to pH 8.2 by HCl.

Preparation of X-shaped DNA and DNA nanospheres

Two types of X-shaped branched DNA (X-DNA) nanostructures were synthesized by mixing the same molar amount of corresponding four single-stranded DNA ($ssDNA_1$, $ssDNA_2$, $ssDNA_3$ and $ssDNA_4$ for X_1, $ssDNA_5$, $ssDNA_6$, $ssDNA_7$ and $ssDNA_8$ for X_2)

with 80 mM NaCl (as shown in **Table S1**), and further going through an annealing procedure by using PCR instruments. DNA nanospheres were formed by simply mixing two types of X-DNA (X_1 and X_2) and target DNA (T-DNA) at the concentration ratio of 1:1:2 at room temperature.

Quartz crystal microbalance (QCM) measurements

All nucleic acid detection procedures were real-time monitored on a dissipative QCM instrument (QSense Initiator, Biolin Scientific, Sweden), and then output as frequency and dissipation signals. The new gold chip (5 MHz) was first immersed in piranha solution (30% H_2O_2, 70% H_2SO_4) at room temperature for 15 min, and then rinsed with water and ethanol, followed by the drying with N_2. Before the QCM measurements, the gold chip was immersed in a solution of H_2O, H_2O_2 and $NH_3 \cdot H_2O$ in a volume ratio of 5:1:1 at 75^{o}C for 5 min. The 0.1 μM capture probe (C-DNA) solution with 1 mM TCEP was shaken at 37^{o}C for 1 h used for the disrupt of disulfide bonds. The treated C-DNA modified with thiol groups were incubated on the clean chip by Au-S bonds at 37^{o}C for 16 h. The chip with C-DNA fixed was blocked with 1 mM 6-mercapto-1-hexanol MCH at 37^{o}C for 1 h to eliminate non-specific adsorption, and then washed with water and ethanol. In a QCM experiment, the temperature was set to 25^{o}C and the flow rate was set to 0.1 mL/min. First, the baseline was leveled by introducing MQ and 1×TE hybridization buffer. And then normal or mutated sequences (N-DNA or M-DNA) and X-DNA was introduced in turn to achieve target recognition and signal amplification,

resulting in the output of real-time frequency and dissipation responses. After a QCM experiment, the chip was regenerated by soaking in 7 M urea solution for 30 min for using in the next QCM measurement. In hybridization thermodynamics and kinetics assays, the temperature was set to 25^{o}C, and pH was set to 8.0.

Thermodynamics and kinetics analysis of TTP system

We studied the thermodynamics and kinetics of DNA hybridization with the first cycle of TTP system as the research object. In these experiments, T-DNA with different concentrations and X_1 were sequentially introduced into the QCM device, and the temperature was set as 25^{o}C. According to the molecular weight and concentration ratio of T-DNA and X_1, we calculated the theoretical ratio of hybridization yield (ρ_T) to be 3.5.

$$\rho_T = \frac{\mathrm{MW}\ (X_1)}{2 \times \mathrm{MW}\ (\text{T-DNA})}$$

where MW (X_1) =63076 g/mol, MW (T-DNA) =9109 g/mol.

Theoretical prediction model

All theoretical values were analyzed by advantage of the website www.nupack.org. The sequences involved in the experiments were used as inputs on the website of www.nupack.org, including normal or mutated DNA sequences, and the sticky ends of two kinds of X-DNA. The theoretical binding energy (Gibbis free energy, ΔG_H) and equilibrium concentrations of hybrid-DNA nanostructures were obtained under the conditions of 25^{o}C, 0.1 M NaCl and 0.1 μM input sequences without dangle treatment,

which were consistent with the experimental conditions. The equilibrium yields (θ) were obtained by calculating the ratio of equilibrium concentrations to the total concentrations.

$$\theta = \frac{\text{equilibrium concentration}}{\text{input concentration}}$$

Hybridization probability (σ) of hybrid-DNA were the results of multiplication of relative binding energy (ΔG_H) and equilibrium yields (θ), which effectively predicted the probability of target hybrid-DNA in a diluted solution.

$$\sigma = \Delta G_H \times \theta$$

Supplemental references

Liu, L., Shou, L., Yu, H., and Yao, J. (2015). Mechanical properties and corrosion resistance of vulcanized silicone rubber after exposure to artificial urine. J Macromol Sci B *54*, 962-974.

Marques, M.R.C., Loebenberg, R., and Almukainzi, M. (2011). Simulated biological fluids with possible application in dissolution testing. Dissolut Technol *18*, 15-28.